Coupling delay controls synchronized oscillation in the segmentation clock

Kumiko Yoshioka-Kobayashi[1,2], Marina Matsumiya[1,3], Yusuke Niino[4], Akihiro Isomura[1,5,6], Hiroshi Kori[7], Atsushi Miyawaki[4,8], and Ryoichiro Kageyama[1,2,3,6]*

[1] Institute for Frontier Life and Medical Sciences, Kyoto University, Kyoto 606-8507, Japan
[2] Graduate School of Medicine, Kyoto University, Kyoto 606-8501, Japan
[3] Graduate School of Biostudies, Kyoto University, Kyoto 606-8501, Japan
[4] Laboratory for Cell Function and Dynamics, Brain Science Institute, RIKEN, 2-1 Hirosawa, Wako-city, Saitama 351-0198, Japan
[5] Japan Science and Technology Agency, PRESTO, Saitama 332-0012, Japan
[6] Institute for Integrated Cell-Material Sciences, Kyoto University, Kyoto 606-8501, Japan
[7] Graduate School of Frontier Sciences, The University of Tokyo, Kashiwa-city, Chiba 277-8561, Japan
[8] Biotechnological Optics Research Team, Center for Advanced Photonics, RIKEN, 2-1 Hirosawa, Wako-city, Saitama 351-0198, Japan

*Correspondence: Ryoichiro Kageyama
Institute for Frontier Life and Medical Sciences
Kyoto University
Shogoin-Kawahara, Sakyo-ku
Kyoto 606-8507
Japan
Tel: +81-75-751-4011
Fax: +81-75-751-4807
E-mail: rkageyam@infront.kyoto-u.ac.jp

Individual cellular activities fluctuate, yet are constantly coordinated at the population level via cell-cell coupling. A notable example is the somite segmentation clock, in which the expression of clock genes, such as *Hes7*, oscillates in synchrony between cells comprising the presomitic mesoderm (PSM)[1,2]. This synchronization depends on the Notch signaling pathway, and inhibiting this pathway desynchronizes oscillations, leading to somite fusion[3-7]. However, how Notch signaling regulates HES7 oscillation synchrony is unknown. Here, we established a live-imaging system using a new fluorescent reporter (Hes7-Achilles) to monitor synchronous HES7 oscillations in the mouse PSM at single-cell resolution. Wild-type cells can rapidly correct for phase fluctuations in HES7 oscillations, whereas absence of the Notch modulator *Lunatic fringe* (*Lfng*) leads to loss of PSM cell synchrony. Furthermore, HES7 oscillations are severely dampened in individual cells of *Lfng*-null PSM. However, when *Lfng*-null PSM cells were completely dissociated, HES7 oscillations showed almost normal amplitudes and periodicity, suggesting that LFNG is mostly involved in cell-cell coupling. Mixed cultures of control and *Lfng*-null PSM cells and optogenetic Notch signaling reporter assay revealed that LFNG delays the signal-sending process of intercellular Notch signaling transmission. These results together with mathematical modeling raised the possibility that *Lfng*-null PSM cells shorten the coupling delay, thereby approaching a condition known as the oscillation/amplitude death of coupled oscillators[8]. Indeed, a small compound, which lengthens the coupling delay, partially rescues the amplitude and synchrony of HES7 oscillations in *Lfng*-null PSM cells. Thus, our study reveals a delay control mechanism of the oscillatory networks involved in somite segmentation, and indicates that intercellular coupling with a proper delay is essential for the synchronized oscillations.

The segmentation clock controls the periodic formation of somites, which are repetitive structures that lie along the body axis and give rise to vertebrae and ribs. The core of this clock system is controlled by cyclic expression of Hes/her genes, such as *Hes7* [9,10], and by periodic activation of the Notch, Fgf, and Wnt signaling pathways in the PSM[1,2]. In mice, *Hes7* expression oscillates with ~2-h periodicity, which defines the pace of segmentation[9]. Individual PSM cells carry their own clock but are coupled to

each other to generate coherent oscillation waves that lead to the formation of segmentation boundaries. This coupling is essential for segmentation, because uncoupling between cells results in severe somite fusion and morphological irregularities[3-7]. The Notch pathway is a critical mediator of this coupling mechanism in various species[1-7]. *Hes7* oscillations drive oscillatory expression of the Notch ligand gene *Delta-like1* (*Dll1*), which affects *Hes7* oscillations in neighboring cells[11,12]. However, *Dll1* alone is not sufficient for synchronous oscillations. In mice, LFNG, a glycosyltransferase for DLL1 and Notch proteins[13], also exhibits oscillatory expression under the control of *Hes7* and is suggested to be a key coupling factor: *Lfng*-knockout (KO) mice exhibit somite segmentation irregularities, as *Hes7* expression becomes asynchronous between PSM cells[14-17]. However, most analyses have been based on fixed samples, and as such, a direct observation of single-cell clock oscillator dynamics is lacking.

Clock gene reporters are powerful tools for studying oscillator dynamics but need more improvement. Our previous imaging analyses with a Hes7 promoter-driven destabilized luciferase reporter (pHes7-UbLuc) allowed for ensemble detection of *Hes7* oscillations with a shorter period and a substantially lower amplitude in *Lfng*-KO PSM than in the wild type (WT) (Extended Data Fig. 1)[16]. The overall attenuation seen in the *Lfng*-KO waveform could possibly result from either a lower amplitude of individual PSM cells' oscillation, desynchronization between PSM cells, or both. To discriminate between these possibilities, it is imperative to quantitatively follow the oscillations in individual PSM cells. A luciferase-based reporter system is not applicable to quantify *Hes7* oscillations in individual cells of the intact PSM because of its limited spatio-temporal resolution. Therefore, we established novel HES7 fluorescent reporter mice. We first produced a HES7 reporter with the fast maturing YFP "Venus"[18], by making a Venus-HES7 fusion protein, but we were not able to obtain sufficient signals for single-cell quantification (n=0/7). Considering the short half-life of HES7 (22.3 min)[19], fusion to this rapidly degraded protein was thought to prevent Venus from synthesizing its chromophore before degradation of the fused protein. We therefore performed directed evolution on the *Venus* gene through successive rounds of mutagenesis, screening, and validation to improve the maturation rate (see Methods). In total, 15 residues were subjected to site-directed random mutagenesis, and subsequently constructed gene libraries were screened by selecting for bacterial colonies with fast

maturation. With 8 amino acid substitutions, we developed a faster-maturing YFP variant, designated Achilles (Extended Data Fig. 2). *In vitro* experiments revealed that Achilles has the same spectral properties and maturation yield as Venus, but that Achilles outperforms Venus in terms of maturation speed (Fig. 1b,c and Extended Data Fig. 2).

We next generated transgenic mice carrying the Hes7 promoter-driven Achilles reporters (Extended Data Fig. 3), which showed higher intensity and oscillation amplitudes in signal detection than Venus. Live imaging of PSM tissues from pHes7-Achilles-Hes7 (Extended Data Fig. 3b, hereafter called Hes7-Achilles reporter), which showed the most similar pattern to the endogenous HES7 protein expression among the tested constructs, successfully captured oscillatory expression at single-cell resolution (Fig. 1a,d, n=2/3). Furthermore, this line rescued *Hes7*-null mice (Extended Data Fig. 4), suggesting that the Achilles-HES7 fusion protein is biologically functional. Cell tracking and signal quantification enabled us to quantify the phase of HES7 oscillation in individual PSM cells over time (Fig. 1e and Extended Data Fig. 5). Using the Hes7-Achilles reporter, we compared HES7 oscillation dynamics between control and *Lfng*-KO mice by culturing whole PSM tissues[16] and tail bud regions[20]. In both control and *Lfng*-KO PSM, each cell exhibited stable oscillation (Fig. 1d,e and videos S1 and S2). Notably, in the control PSM, HES7 expression oscillated synchronously between neighboring cells (Figs. 1d,e and 2a). Phase fluctuation sometimes occurred, probably due to cell division and migration, but this was immediately corrected in the control, such that synchrony was restored by the next cycle (Fig. 2a). By contrast, individual *Lfng*-KO cells showed a smaller amplitude, a shorter period, and more phase fluctuation than control cells in the PSM (Figs. 1d,e and 2a-c, and videos S1 and S2). The averaged HES7 expression levels decreased in the anterior *Lfng*-KO PSM compared to the control (Fig. 2d). We also assessed the degree of synchronization between oscillators by measuring the mean phase coherence (using the Kuramoto order parameter)[21], which showed that *Lfng*-KO PSM cells have a lower synchronization rate than control cells (Fig. 2e,f). We also performed tail bud cultures and found milder but similar defects in *Lfng*-KO (Extended Data Fig. 6). Similar defects were observed in another independent line of Hes7-Achilles reporter mice (Extended Data Fig. 6d-g). Furthermore, both acute inhibition of Notch signaling (+DAPT) and acute knock-down of *Lfng* gradually led to similar defects in the control tail bud cultures (Extended Data

Fig. 7a-f), as observed in Notch signaling mutants[3]. These data indicate that a lower amplitude at the population level in *Lfng*-KO PSM originates from both lower amplitudes in individual cells and reduced synchronization across cells.

To address whether the lower amplitude in *Lfng*-KO PSM arises from a lower amplitude of intrinsic oscillation or a coupling process, we examined Hes7-Achilles reporter expression in single isolated cells that had no interactions with their neighboring cells. In these single-cell dissociation cultures (Fig. 2g)[22], HES7 oscillations were independent of Notch signaling (Extended Data Fig. 7g,h). Under this condition, both control and *Lfng*-KO PSM cells maintained stable oscillations with similar periodicity and only slightly different amplitudes (~10% smaller in *Lfng*-KO) (Fig. 2h-k). Because the oscillation amplitude did not markedly differ between control and *Lfng*-KO dissociated cells, the substantially smaller amplitudes detected in the intact *Lfng*-null PSM (Fig. 2c) likely result from abnormal cell-cell coupling through Notch signaling.

To understand the role of LFNG in Notch signaling-mediated cell-cell coupling, we directly assessed how oscillations are affected in WT/*Lfng*-KO mixed cell cultures by using the Hes7-Achilles reporter. When a small ratio (1:20) of WT cells were mixed into the *Lfng*-KO cell population (WT in *Lfng*-KO), the WT cells expressed a normal level of HES7 and maintained roughly the same pace as *Lfng*-KO cells (Fig. 3b, middle panel). The accuracy was decreased in this condition (Fig. 3b, right panel) compared with WT-to-WT cell coupling (Fig. 3a), but this is most likely due to the fluctuation of inputs from neighboring *Lfng*-KO cells. Thus, DLL1 signals from *Lfng*-KO cells were transmitted to WT cells. However, WT cells exhibited ~0.25π (corresponding to ~15 min) advance in peak phase compared to *Lfng*-KO cells (Fig. 3b, right panel). This phase advance in WT cells compared to *Lfng*-KO cells indicated that DLL1-Notch signal transmission from *Lfng*-KO cells is faster than that from WT cells, suggesting that the absence of LFNG shortens the Notch signaling-sending process. By contrast, when mixing a small ratio (1:20) of *Lfng*-KO cells into a WT population (*Lfng*-KO in WT), HES7 oscillations in *Lfng*-KO cells showed lower amplitudes and did not keep phase well with WT cells, indicating that *Lfng*-KO cells did not respond properly to DLL1 signals from WT cells (Fig. 3c), suggesting that LFNG regulates the amplitude of HES7 oscillations in the Notch signaling-receiving process. These data indicate that LFNG has dual functions: delaying the signal-sending process and increasing the

amplitude in the signal-receiving process.

The coupling observed in "WT in *Lfng*-KO" but not in "*Lfng*-KO in WT" could be due to asymmetric coupling of PSM cells, in which faster oscillators (such as *Lfng*-KO) can accelerate slower oscillators (such as WT), whereas slower oscillators cannot decelerate faster oscillators. To exclude this possibility, WT PSM cells were co-cultured with mutant PSM cells that exhibited faster HES7 oscillation by deletion of two introns from the *Hes7* gene (In(3), Extended Data Fig. 8)[23]. This analysis showed that slower WT oscillators can decelerate a small ratio (1:20) of faster mutant oscillators (Extended Data Fig. 8b), indicating that the phase advance in "WT in *Lfng*-KO" is not due to asymmetric coupling.

We further examined the role of Lfng in Notch signaling-mediated cell-cell coupling by using the recently developed optogenetic sender-receiver system[12]. In this system, the Notch ligand DLL1 expression is optogenetically induced in sender cells, while the response in receiver cells is monitored using a *Hes1* reporter (Fig. 4a)[12]. In these cells, endogenous *Hes1* expression oscillates with ~2-h periodicity, like *Hes7* oscillations in the PSM[12]. Sender and receiver cells were co-cultured, and after optogenetic induction of *Dll1* expression, *Hes1* reporter expression in receiver cells was monitored using photo-multiplier tubes. The presence of LFNG in DLL1 signal-sending cells increased the time required for the *Hes1* response (Fig. 4b, upper panel, compare lanes 1 and 2 or lanes 4 and 5, and Fig. 4c) and decreased the amplitude in receiver cells (Fig. 4b, lower panel). The delayed *Hes1* response was almost the same irrespective of whether *Lfng* expression was sustained or oscillatory (Fig. 4b, upper panel, compare lanes 2 and 3 or lanes 5 and 6). We also found that the transport of DLL1 protein to the cell surface was delayed by ~15 min in the presence of *Lfng* compared to the absence of *Lfng* (Fig. 4d-h). However, the half-life of DLL1 protein was not affected by LFNG (Fig. 4i). By contrast, LFNG in receiver cells did not affect the delay (Fig. 4b, upper panel, compare lanes 1 and 4), but increased the amplitude of the *Hes1* response (Fig. 4b, lower panel, compare lanes 1 and 4). Thus, LFNG increases both the delay in the signal-sending process and the amplitude in the signal-receiving process, agreeing well with the above WT/*Lfng*-KO mixed cell culture experiments.

Mathematical modeling (Extended Data Fig. 9a-c) suggests that the coupling delay (τ_2), the time required for *Hes7* from one cell to repress *Hes7* in its neighboring cell, is very important for dynamics of in-phase oscillations[11,24,25]. When this delay is decreased

or increased, the in-phase oscillations are severely dampened, disrupting cell-cell synchrony (Extended Data Fig. 9d, compare τ_2 = 1.0 with other τ_2 values) and approaching a condition known as amplitude/oscillation death (Extended Data Fig. 9e)[8], whereby the expression becomes steady (non-oscillatory). We speculate that by increasing the time required for intercellular DLL1-Notch signal transmission, LFNG may adjust the coupling delay to make it suitable for robust in-phase oscillations. It was shown that expression level of the Notch intracellular domain (NICD), which is formed upon activation of Notch signaling, oscillates in the PSM dependently on *Lfng*[16,17,26,27], and that sustained expression of *Lfng* down-regulates endogenous *Lfng* expression[28], suggesting that LFNG is involved in the down-regulation of Notch signaling. However, the average levels of HES7 expression decreased in the anterior *Lfng*-null PSM (Fig. 2d). Furthermore, it was shown that sustained *Lfng* expression does not abolish cyclic expression of endogenous *Hes7* in the PSM[29]. Thus, the repressor role of *Lfng* in the PSM remains obscure, and our data suggested that LFNG does not inhibit Notch signaling but increases the amplitude and the coupling delay (Fig. 4b).

To address the significance of the coupling delay in synchronized oscillations, we performed chemical library screening with ES cell-derived PSM-like tissues[30] to search for small molecules that could ameliorate the *Lfng*-KO phenotype. Because the coupling delay decreased in the absence of *Lfng*, chemicals that increase the coupling delay may at least partially rescue the *Lfng*-KO phenotype. Such chemicals would slightly increase the period of HES7 oscillations in WT cells (Extended Data Fig. 9e), although mechanisms other than the coupling delay could also affect the oscillatory period. We screened 431 compounds targeting mainly signaling and gene regulation and found that 26 of them increased the period of *Hes7* oscillations more than 10 min in ES cell-derived PSM-like tissues (Supplementary Table S1). Interestingly, two of them, Norcantharidin and Kenpaullone, regulate Wnt signaling, which is known to have cross-talk with Notch signaling[1,2]. Thus, we analyzed additional Wnt signaling regulators and found that KY02111 (N-(6-Chloro-2-benzothiazolyl)-3,4-dimethoxybenzene-propanamide), Kenpaullone, IWR-I, and C59 increased the coupling delay in the optogenetic sender-receiver system (Extended Data Fig. 10a,b). However, Kenpaullone significantly decreased the amplitude, but the others did not (Extended Data Fig. 10c). Among these compounds, KY02111 did recover the amplitude and synchrony of HES7 oscillations of *Lfng*-KO

PSM cells to some extent (Extended Data Fig. 10d-g), suggesting that this compound can partially rescue the amplitude and synchrony of HES7 oscillations in *Lfng*-KO PSM cells by lengthening the coupling delay.

In summary, we have established a powerful live-cell imaging method that enables quantification of oscillatory dynamics with single-cell resolution. Using this method, we have demonstrated how a phase delay can affect collective dynamic oscillatory gene expression. While pulsatile expression of the Notch ligand DLL1 can incompletely entrain oscillations in neighboring cells[12], the synchrony critically depends on the coupling delay (Extended Data Fig. 9e)[11]. Our findings showed that LFNG is a key coupling factor that may make the delay of intercellular DLL1-Notch signal transmission suitable for robust synchronous oscillation. Furthermore, because *Lfng* mutations cause spondylocostal dysostosis, our study also raised the possibility that small compounds that correct the coupling delay can be used for treatment of such human congenital diseases.

References

1. Hubaud, A. & Pourquié, O. Signalling dynamics in vertebrate segmentation. *Nat. Rev. Mol. Cell Biol.* **15***,* 709-721 (2014).
2. Oates, A.C., Morelli, L.G. & Ares, S. Patterning embryos with oscillations: structure, function and dynamics of the vertebrate segmentation clock. *Development* **139***,* 625-639 (2012).
3. Jiang, Y.-J. *et al*. Notch signalling and the synchronization of the somite segmentation clock. *Nature* **408**, 475-479 (2000).
4. Riedel-Kruse, I.H., Müller, C. & Oates, A.C. Synchrony dynamics during initiation, failure, and rescue of the segmentation clock. *Science* **317**, 1911-1915 (2007).
5. Mara, A., Schroeder, J., Chalouni, C. & Holley, S.A. Priming, initiation and synchronization of the segmentation clock by deltaD and deltaC. *Nat. Cell Biol.* **9**, 523-530 (2007).
6. Özbudak, E.M. & Lewis, J. Notch signalling synchronizes the zebrafish segmentation clock but is not needed to create somite boundaries. *PLoS Genet.* **4**, e15 (2008).

7. Delaune, E.A., François, P., Shih, N.P. & Amacher, S.L. Single-cell-resolution imaging of the impact of Notch signaling and mitosis on segmentation clock dynamics. *Dev. Cell* **23**, 995-1005 (2012).
8. Ramana Reddy, D.V., Sen, A. & Johnston, G.L. Experimental evidence of time delay induced death in coupled limit cycle oscillators. *Phys. Rev. Lett.* **80,** 5109-5112 (1998).
9. Bessho, Y. *et al*. Dynamic expression and essential functions of *Hes7* in somite segmentation. *Genes Dev.* **15**, 2642-2647 (2001).
10. Sparrow, D.B., Guillén-Navarro, E., Fatkin, D. & Dunwoodie, S.L. Mutation of *HAIRY-AND-ENHANCER-OF-SPLIT-7* in humans causes spondylocostal dysostosis. *Hum. Mol. Genet.* **17,** 3761-3766 (2008).
11. Shimojo, H. *et al*. Oscillatory control of Delta-like1 in cell interactions regulates dynamic gene expression and tissue morphogenesis. *Genes Dev.* **30**, 102-116 (2016).
12. Isomura, A., Ogushi, F., Kori, H. & Kageyama, R. Optogenetic perturbation and bioluminescence imaging to analyze cell-to-cell transfer of oscillatory information. *Genes Dev.* **31**, 524-535 (2017).
13. Moloney, D. J. *et al.* Fringe is a glycosyltransferase that modifies Notch. *Nature* **406,** 369–375 (2000).
14. Evrard, Y.A., Lun, Y., Aulehla, A., Gan, L., & Johnson, R.L. *lunatic fringe* is an essential mediator of somite segmentation and patterning. *Nature* **394,** 377-381 (1998).
15. Zhang, N. & Gridley, T. Defects in somite formation in lunatic fringe-deficient mice. *Nature* **394,** 374-377 (1998).
16. Niwa, Y. *et al*. Different types of oscillations in Notch and Fgf signaling regulate the spatiotemporal periodicity of somitogenesis. *Genes Dev.* **25**, 1115-1120 (2011).
17. Okubo, Y. *et al*. Lfng regulates the synchronized oscillation of the mouse segmentation clock via trans-repression of Notch signalling. *Nat. Commun.* **3**, 1141 (2012).
18. Nagai, T. *et al*. A variant of yellow fluorescent protein with fast and efficient maturation for cell-biological applications. *Nat. Biotechnol.* **20**, 87-90 (2002).
19. Hirata, H. *et al*. Instability of Hes7 protein is critical for the somite segmentation clock. *Nat. Genet.* **36**, 750-754 (2004).

20. Lauschke, V.M., Tsiairis, C.D., François, P. & Aulehla, A. Scaling of embryonic patterning based on phase-gradient encoding. *Nature* **493,** 101-105 (2013).
21. Pikovsky, A., Rosenblum, A. & Kurths, J. Synchronization. *Cambridge University Press* (2001).
22. Hubaud, A., Regev, I., Mahadevan, L. & Pourquié, O. Excitable Dynamics and Yap-dependent mechanical cues drive the segmentation clock. *Cell* **171,** 668-682 (2017).
23. Harima, Y., Takashima, Y., Ueda, Y., Ohtsuka, T. & Kageyama, R. Accelerating the tempo of the segmentation clock by reducing the number of introns in the *Hes7* gene. *Cell Rep.* **3,** 1-7 (2013).
24. Lewis J. Autoinhibition with transcriptional delay: a simple mechanism for the zebrafish somitogenesis oscillator. *Curr. Biol.* **13,** 1398-1408 (2003).
25. Morelli, L.G., Ares, S., Herrgen, L., Schröter, C., Jülicher, F. & Oates, A.C. Delayed coupling theory of vertebrate segmentation. *HFSP J.* **3**, 55-66 (2009).
26. Morimoto, M., Takahashi, Y., Endo, M. & Saga, Y. The Mesp2 transcription factor establishes segmental borders by suppressing Notch activity. *Nature* **435,** 354-359 (2005).
27. Huppert, S.S., Ilagan, M.X., De Strooper, B. & Kopan, R. Analysis of Notch function in presomitic mesoderm suggests a γ-secretase-independent role for presenilins in somite differentiation. *Dev. Cell* **8,** 677-688 (2005).
28. Williams, D.R., Shifley, E.T., Braunreiter, K.M. & Cole, S.E. Disruption of somitogenesis by a novel dominant allele of *Lfng* suggests important roles for protein processing and secretion. *Development* **143,** 822-830 (2016).
29. Serth K, Schuster-Gossler K, Cordes R, & Gossler A. Transcriptional oscillation of Lunatic fringe is essential for somitogenesis. *Genes Dev.* **17,** 912-925 (2003).
30. Matsumiya, M., Tomita, T., Yoshioka-Kobayashi, K., Isomura, A. & Kageyama, R. ES cell-derived presomitic mesoderm-like tissues for analysis of synchronized oscillations in the segmentation clock. *Development* **145,** dev156836 (2018).

Acknowledgements

We thank Caroline Vissers for critical reading, Risa Sueda for technical help, Fumiyoshi Ishidate for live imaging, Hitoshi Miyachi for generation of transgenic mice, and Motonari Uesugi for providing KY02111. This work was supported by Core

Research for Evolutional Science and Technology (JPMJCR12W2 to R.K.), Precursory Research for Embryonic Science and Technology (to A.I.), Grant-in-Aid for Scientific Research on Innovative Areas (Ministry of Education, Culture, Sports, Science, and Technology (MEXT), Japan (16H06480 to R.K.; 15H05876 to H.K.), and the Brain Mapping by Integrated Neurotechnologies for Disease Studies (Brain/MINDS) (JP19dm0207001 to A.M.).

Author contribution

K.Y.-K. developed Hes7 reporter mice, performed the experiments, analyzed the data, and wrote the manuscript; M.M. performed chemical library screening; A.I. analyzed the data; Y.N. and A.M. developed Achilles, analyzed the data, and wrote the manuscript; H.K. performed mathematical modeling analysis; R.K. designed and supervised the project and wrote the manuscript.

Author Information

The authors declare no competing financial interests.

Figure legends

Figure 1. Characterization of Achilles and analysis of Hes7-Achilles oscillations in control and *Lfng*-KO mice. a. Structure of the Achilles-Hes7 transgene. Achilles-HES7 fusion protein expression was quantified and calculated for oscillation phase mapping in each PSM cell. **b.** Excitation (broken)/emission (solid) spectra of Achilles (red) and Venus (black). **c.** Time course of fluorescence intensities of Achilles (red) and Venus (black) synthesized from their mRNAs by the PURE system (mean values ± SEM from three experiments). **d.** Live imaging of the Hes7-Achilles reporter in WT and *Lfng*-KO PSM by confocal microscopy. Z-projection images of the maximum intensity are shown. Signals were obtained at the single-cell resolution. The schema indicates the orientation of the PSM. **e.** Single-cell analysis of WT and *Lfng*-KO PSM. *left,* HES7 phase distribution in WT and *Lfng*-KO. *right,* Fluorescence and phase time-series from 10 randomly selected cells in the posterior part of WT and *Lfng*-KO PSM. Scale bars, 100μm.

Figure 2. Loss of *Lfng* affects oscillation period, amplitude and synchronization.

HES7 oscillations were examined in intact PSM tissues (**a-f**) and dissociated PSM cells (**g-k**). WT (**a-f**) or *Lfng*(+/–) (**h-k**) PSM cells were used as controls. **a.** cos θ plots of single-cell time-series in control and *Lfng*-KO PSM. Each row corresponds to one cell. Tracks are aligned based on average position along the antero-posterior axis. The HES7 expression domain was divided into 5 positions, and positions 2 and 5 in the schema were used for quantification of the anterior and posterior PSM, respectively (**b-f**). **b.** Oscillation period from Hes7-Achilles fluorescence time-series in single PSM cells. **c.** Oscillation amplitude from Hes7-Achilles fluorescence time-series in single PSM cells. **d.** Average expression levels of Hes7-Achilles fluorescence in single PSM cells. At least 190 cells were examined for each genotype. Error bars indicate SEM. ***$p<0.001$, ****$p<0.0001$, unpaired *t* test. **e.** Phase distribution at the 1st peak timing of average signals in the posterior and anterior PSM. At least 100 cells were examined for each genotype. *$p<0.05$, ***$p<0.001$, ****$p<0.0001$, Rayleigh test. **f.** Kuramoto order parameter calculated using phase shown in **e**. Error bars indicate SEM. *$p<0.05$, unpaired *t* test. **g.** Tail bud tissue was cultured for 24 h before dissociation. After dissociation, cells were cultured on Fibronectin-coated plates in the presence of 0.5μM Latrunculin A. Scale bars, 100μm. **h.** Examples of Hes7-Achilles signals from ROIs in dissociation cultures of PSM cells. **i.** Examples of Hes7-Achilles signals in dissociation culture of PSM cells. **j.** Oscillation period of Hes7-Achilles fluorescence in dissociated PSM cells. **k.** Oscillation amplitude from Hes7-Achilles fluorescence in dissociated PSM cells. At least 100 cells were examined for each genotype. Error bars indicate SEM. *$p<0.05$, unpaired *t* test.

Figure 3. Loss of *Lfng* affects timing information in cell-cell signal transmission. a. WT PSM cells expressing Achilles-Hes7 and those expressing both Achilles-Hes7 and H2B-mCherry were mixed at a 20:1 ratio. **b.** WT (white) PSM cells were mixed as a minority in *Lfng*-KO cells (pink) in a 1:20 ratio. **c.** *Lfng*-KO PSM cells (pink) were mixed as a minority in WT cells (white) in a 1:20 ratio. Fluorescence was quantified over time in the minority and majority cells. Only representative cells as well as the population average are shown (middle panels). The distribution of phase difference between the minority cells and their neighboring cells was calculated at each time point (right panels). At least 150 minority cells were examined in 4 independent experiments for each mixture. ****$p< 0.0001$, Rayleigh test.

Figure 4. LFNG in sending cells lengthened the time required for *Hes1* response to DLL1. a. C2C12 myoblast sender cells carried the hGAVPO-based optogenetic Dll1-inducible system, while C2C12 myoblast receiver cells carried the Hes1-UbLuc2 reporter[12]. These cells were co-cultured, and *Hes1* reporter expression was monitored after light-induction of DLL1. **b.** (Upper) Averages of peak-timings in *Hes1* reporter signals were compared between receiver cells with and without *Lfng*. (Lower) Averages of amplitude in *Hes1* reporter signals divided by mean signal intensity were compared between sender/receiver cells with and without *Lfng*. Oscillatory *Lfng* (Light-inducible *Lfng*) expression was also induced in sender cells. n≥20 for each combination. **c.** Representative time-series of *Hes1* reporter signal in receiver cells co-cultured with sender cells expressing *Dll1* with or without *Lfng*. **d.** DLL1-Luc2 fusion protein was expressed in C2C12 cells with or without *Lfng* using hGAVPO-based optogenetic inducible system. Golgi-mCherry-2a-mem-iRFP670 was also expressed as markers for image segmentation. **e.** DLL1-Luc2 expressing cells were co-cultured with WT C2C12 cells at 1:4 ratios. Luminescence, iRFP670, and mCherry signals were imaged with CCD camera after blue-light illumination. Snapshots of cells from multi-color imaging are shown. Scale bar: 50 μm. **f.** Representative time-series of DLL1-Luc2 images after light pulse. Scale bar: 50 μm. **g.** Normalized DLL1-Luc2 signals at plasma membrane ($iRFP^+$;$mCherry^-$) after light pulse. **h.** Peak-timings of DLL1-Luc2 signals after light pulse. Average peak-timing from 3 independent experiments are shown. **i.** Half-life of DLL1-Luc2 in the presence or absence of *Lfng*. Average half-life from three independent experiments is shown. Error bars indicate SEM. *p<0.05, **p<0.01, ***p<0.001, unpaired t test.

METHODS

Generation of Achilles

Venus[18] was used as a starting template for PCR-based site-directed and semi-random mutagenesis with degenerate primers. Amplified cDNAs were subcloned in-frame into the *Bam*HI/*Eco*RI sites of $pRSET_B$ and constructed vectors were transformed into *E. coli* JM109(DE3). Colonies were screened for fluorescence using a transilluminator. Fifteen positions (Ser-30, Tyr-39, Gln-69, Cys-70, Ile-128, Asp-129, Tyr-145, Asn-146, Ser-147, His-148, Lys-166, Ile-167, Arg-168, His-169 and Ala-206) were investigated and a variant with Arg-30, Ile-39, Ala-69, Val-70, Ser-128, Gly-129, Phe-145 and Phe-206 was chosen as Achilles. The nucleotide sequence reported in this paper has been deposited in the DDBJ/EMBL/GenBank under an accession number, LC381432 (Achilles).

In vitro characterization of fluorescent proteins

JM109(DE3) cells expressing His-tagged fluorescent proteins were grown at 37°C on a rotary shaker at 180 rpm for 17 h in LB medium. The bacteria were collected and resuspended in PBS with 10 mg/mL lysozyme and protease inhibitors (10 μM E-64, 10 μM leupeptin and 1 μM pepstatin A) and lysed by freeze-thaw cycling and sonication. Protein purification from the supernatant was carried out using Ni-NTA agarose, followed by buffer exchange into 50 mM HEPES-KOH (pH = 7.4) using a PD-10 column (GE Healthcare). Absorption and fluorescence spectra were measured using a spectrophotometer (U-3310, Hitachi) and a multi-mode microplate reader (Synergy Mx, BioTek), respectively. Molar extinction coefficient was calculated with protein concentrations measured using a Bradford protein assay kit (Bio-Rad) with BSA as the standard. Absolute fluorescence quantum yields were measured using an integrating sphere (C9920, Hamamatsu) with a multi-channel analyzer (C10027, Hamamatsu). A pH titration experiment was performed using buffers containing 25 mM of acetate (pH 4.0, 4.5, 5.0), MES (pH 5.5, 6.0, 6.5), HEPES (pH 7.0, 7.5, 8.0) or borate (8.5, 9.0, 9.5, 10.0).

Imaging of bacterial colonies

Time-lapse imaging of transformed *E. coli* colonies was carried out using our homemade fluorescence analyzing system consisting of a Xenon light source

(MAX-301, Asahi Spectra) and a cooled CCD camera (CoolSNAP HQ, Photometrics) controlled by MetaMorph (Universal Imaging). 480AF30 (Omega Optical) and PB0540/020 (Asahi Spectra) filters were used for excitation and emission, respectively. The same amount of competent JM109(DE3) cells was used for transformation with the $pRSET_B$-Achilles and $pRSET_B$-Venus genes. After 3 h incubation at 37°C the plate was placed in a stage-top incubation chamber (IBC, Tokai Hit) kept at 37°C and time-lapse imaging was immediately started. Images were analyzed using ImageJ (National Institutes of Health) and the 5-parameter sigmoidal curve [SigmaPlot (Systat Software)] gave the best fit curve for the time course data.

Fluorescence measurement of synthesized proteins

Achilles and Venus cDNAs were inserted into the *Bam*HI/*Eco*RI sites of pCS2 with a partial Kozak sequence CCACCATGG. The plasmids were linearized with *Not*I and mRNAs were synthesized using an mMESSAGE mMACHINE SP6 kit (Ambion). Protein synthesis was started by adding the synthesized mRNA to a cell-free protein-synthesizing system (PURE*frex* 2.0, Gene Frontier)[31]. The reaction mixture was placed in a microplate reader (Synergy Mx, BioTek) at 37 °C and the fluorescence was monitored with excitation and emission wavelengths at 480 nm and 530 nm, respectively. The 5-parameter sigmoidal curve [SigmaPlot (Systat Software)] gave the best fit curve for the time course data.

Generation of pHes7-Achilles reporter transgenic mice

The reporter construct design was drawn in Extended Data Fig. 3. Venus-Hes7 and Achilles-Hes7 transgenes were generated as follows. The XhoI-Kozak-Venus-Hes7 fragment was amplified by PCR, and then inserted between the genomic fragment of the Hes7 promoter and the 3' UTR region, which were used in the pHes7-UbLuc transgene[32]. Transgenic mice were generated by injecting the linearized constructs without backbone sequences into the ICR pronuclei of fertilized eggs. All animals were handled in accordance with the Kyoto University Guide for the Care and Use of Laboratory Animals. Genotyping was performed using the following primers: forward, 5'-CGACC ACTAC CAGCA GAACA-3'; reverse, 5'-ATCCT CACTC CTAGT CCACA GAG-3'.

Explant culture

Male mice carrying Hes7-Achilles Tg were mated with wild-type ICR females, and then females at day 10 of pregnancy were sacrificed. For live imaging aimed for cell tracking and subsequent single-cell quantification, Achilles-Hes7 Tg mice were crossed with ROSA26-H2B-mCherry line mice[33]. Embryos were dissected out in DMEM/F12 with 15mM HEPES (Gibco) supplemented with 100 units/ml penicillin, 100 μg/ml streptomycin (Nacalai Tesque) and 0.2% BSA (Sigma). Culture medium for whole PSM tissues consists of DMEM/F12 (Cell Culture Technologies) plus 1%BSA, 2mM L-glutamine (Gibco), 1g/L glucose (Wako) and 15mM HEPES (Nacalai Tesque). For whole PSM cultures, tail regions including PSM and 2-3 formed somite pairs were embedded in 0.15% (for wide field) or 0.3% (for confocal) low-melting-point agarose (SeaPlaque GTG, FMC) diluted in culture medium. The gel was set in a silicon ring attached onto a 35-mm glass-bottom dish (ø14-mm, Matsunami). Culture medium for tail buds was CO_2 5%-equilibrated DMEM/F12 (Cell Culture Technologies) plus 1%BSA, 2mM L-glutamine, 0.1g/L glucose without HEPES, which was basically the same as previously established[20]. For tail bud culture, a glass-bottom dish was coated with Fibronectin 50μg/mL (Sigma) diluted in PBS for 2 h on a 35°C hot plate. Tail bud regions were excised and put onto a Fibronectin-coated glass bottom dish with the anterior side down. Whole PSM tissues and tail bud explants were maintained in a humidified chamber at 37˚C in 5% CO_2 and 80% O_2, or in 5% CO_2, respectively. To perturb Notch signaling, 5μM DAPT treatment or acute knockdown of *Lfng* was performed.

For acute knockdown of *Lfng*, two shRNA targeting mouse *Lfng* mRNA (shLfng-1: GCATAGCCTCTCCGAGTACTTTCAAGAGAAGTACTCGGAGAGGCT ATGCTTTT; shLfng-2: CCCCTGAGCTATGGCATGTTTGAGAATCAAGAGTTCTC AAACATGCCATAGCTCAGGGTTTT) and scrambled shRNA (GCCCGTTATCGCAC TGATTCATCAAGAGTGAATCAGTGCGATAACGGGCTTTT) were designed and inserted downstream of human U6 promoter. pPGK-iRFP670-NLS expression cassette was also attached to monitor transfected cells. For electroporation and subsequent imaging, tail bud tissues from E10 embryos carrying Hes7-Achilles transgene and ROSA26-H2B-mCherry allele were used and cultured following a previously

established explant culture method[22]. Tail bud mesenchyme cells were isolated, placed into an electrode chamber (CUY505P5, NEPAGENE) filled with 1μg/ml shRNA-expression plasmid diluted with Opti-MEM (Thermo Fisher Scentific) and then incubated for 10 min at room temperature. Two successive poring pulses of 100 V for 5 msec and five successive transfer pulses of 20 V for 50 msec were applied using NEPA21 Super Electroporator (NEPAGENE). Tissues were then transferred onto Fibronectin-coated glass-bottom dish. Time-lapse imaging was started after 6 h of incubation at 37°C in 5% CO_2.

Live imaging

Confocal imaging was performed on a Zeiss LSM780 upright (for whole PSM culture), or inverted (for tail bud culture) laser-scanning microscope. A 20x water immersion lens and a 40x oil immersion lens were used for whole PSM culture and tail bud culture, respectively. Achilles was excited with a 514nm Argon laser. Additionally, for multi-color imaging aimed for cell tracking, mCherry was excited with a 561-nm diode-pumped solid-state laser. A Z-stack of 20-30 images was taken with 2-3-μm depth intervals every 180 sec (for whole PSM) or 90 sec (for tail bud). Multicolor imaging was performed by simultaneous excitation using a 514/561-nm laser with 458/514/561/633-nm main beam splitter. Wide field live imaging was performed either on an Olympus IX81 equipped with a cooled charge-coupled device (CCD) camera (Princeton Instruments Trenton, NJ, VersArray 1 kb) or an Olympus IX83 equipped with an iKon-M (Andor) CCD camera. Signals from samples were collected by an Olympus (Tokyo) ×10 UPlanApo objective. For bioluminescence imaging, 1mM D-Luciferin (Nacalai Tesque) was added to culture medium. Signal-to-noise ratios were increased by 4 × 4 binning and 3-min exposure.

Image processing, cell-tracking and signal quantification

For confocal images, the mCherry channel was used for cell tracking and signal normalization. Raw images were smoothed by Savitzky-Golay temporal filter with 5-frame window size and subjected to tracking by TrackMate[34] in Fiji/ImageJ. Parameters such as mean intensity and position in xyz directions for each cell at each time frame were taken from a 6-μm diameter circle at the center of each cell. Further signal analysis was performed with custom-made programs in Matlab. Mean intensity in

Achilles channel was divided by mCherry intensity for normalization. To de-trend time-series data, a trend line was drawn by taking the moving average of the signal with a window size of 240 min and then subtracted from normalized signal. Savitzky-Golay filtering with 3rd order and window size 60-80 min was applied to smooth the signal. Hilbert transform was performed to obtain instantaneous oscillation phase. Period and amplitude were quantified by peak-detection on de-trended/smoothed intensity. The definition of amplitude was the same as described previously[35]. For bioluminescence imaging, spike noise induced by cosmic ray was removed. Spatio-temporal pattern was obtained by averaging signal along left-to-right axis for each time point and aligned in temporal sequence.

Quantification of synchronization and statistical analysis

To evaluate whether a population of oscillators were synchronized, we applied the Rayleigh test to the phase distributions constructed from the single-cell traces of the phase information, as previously described[12]. Oscillation dynamics of population averages were quantified by taking the average signal in the whole area, and processing this signal in the same as single-cell data to obtain instantaneous phase. Relative phase-shift from collective oscillation for each cell was quantified by calculating phase difference between neighboring cell phase and single-cell phase. To compare the synchronization efficiency, Kuramoto order parameter was determined, as previously described[21]. The order parameter was calculated using relative phase shift. Anisotropy of phase data was assessed by Rayleigh test.

Mixture experiments

A posterior half of PSM was dissociated mechanically by pipetting up to 30 times, filtered through 10-μm pore cell strainer, and seeded into silicon ring with 1.5-mm diameter and 2-mm height set in a glass-bottom dish coated with Fibronectin. Majority cells carrying Achilles-Hes7 and minority cells expressing both Achilles-Hes7 and H2B-mCherry were mixed at a 20:1 ratio. Cells were maintained in culture medium used in tail bud culture plus 10μM Y-27632 (Wako). Oscillation phase in minority and majority cells were quantified by Hes7-Achilles signal in mCherry-positive or –negative area, respectively.

Single-cell isolation culture

We followed methods described previously[22] with some minor modifications. Tail bud regions were treated in Accutase (Nacalai Tesque) for 5 min on a 35°C hot plate, and ectodermal tissues were removed using a tungsten needle. Explant tissue was cultured on Fibronectin-coated chamber cover glass (Lab-Tek) for 24 h in explant medium consisting of DMEM 4.5 g/L Glucose (Thermo Fisher #31053) plus 15% FCS (Embryonic stem cell-screened, Hyclone), 2mM L-Glutamine (Gibco), 100U Penicillin/100mg/ml Streptomycin (Nacalai Tesque), 1x non-essential amino acid (Gibco), 10mM HEPES (Nacalai Tesque), 0.1mM of β-mercaptoethanol (Gibco), 3μM Chir-99021 (Sigma #SML1046), 200nM LDN-193189 (StemRD #LDN-02), 2.5μM BMS-493, 50ng/mL mFGF4 (R&D), 1mg/mL Heparin (Sigma) and 10μM Y-27632 (Wako). Explant tissue was then detached using a P20 tip, collected in a 1.5-ml tube and then dissociated by pipetting, filtered through 10-μm cell strainer, seeded onto 1% BSA-coated chamber cover glass, and maintained in explant medium plus 0.5μM Latrunculin A (Wako #125-04363).

C2C12 sender/receiver assay

C2C12 cells with a light-inducible *Dll1* (sender) and pHes1-NLS-UbLuc reporter (receiver) were established previously[12]. Various sender/receiver lines were newly established by introducing constructs with *Lfng* expression cassettes listed below into the original sender or receiver line. All plasmids were based on the Tol2 transposon vector system (a gift from the Kawakami Lab). To establish stable cell lines, 0.5μg pCAGGS-mT2TP, 0.125μg pKYK34-pEFs-Puro and 0.375μg pKYK28-pPGK-Dll3-HA-pPGK-iRFP670-NLS or pKYK29-pPGK-Dll3-HA-pPGK-iRFP670-NLS-pPGK-Lfng-Flag was transfected into original sender (S0) or receiver (R0) line cultured in a 12-well plate at 5 x 10^4 cell density using ViaFect transfection reagent (Promega). Cells were expanded and selected by 2μg/ml puromycin for one week. iRFP670-positive cells were then sorted using FACSAria III (BD Biosciences). 1.25 x 10^5 of sender cells and 0.25 x 10^5 of receiver cells were mixed and plated onto black 24-well plates, and photon-counting measurements were performed every 3 min with 5-sec blue light exposure. Light stimuli were applied every 2.5 h with 30 sec duration. Recorded traces were de-trended and then smoothened by a Savitzky-Golay filter.

Time-lapse imaging of DLL1-Luc2 fusion protein in C2C12

C2C12 cells carrying the light-inducible DLL1-Luc2 fusion protein system and the *Dll3* and Golgi-mCherry-2a-mem-iRFP670 expression system with or without the *Lfng* expression vector were established, and the luciferase activity in $iRFP^{+}$;$mCherry^{-}$ regions was quantified.

ES cell-derived PSM-like tissue culture and chemical library screening

PSM-like tissues (iPSM colonies) were induced from mouse ES cells carrying the Hes7-UbLuc reporter, as previously described[30]. A single iPSM colony per well was cultured in gelatin-coated black 24-well plates, and each small compound was added from day 4 onward. *Hes7* promoter-driven luciferase activity was measured by a highly sensitive photo-multiplier tube[36]. Small compounds that lengthened the period of *Hes7* oscillations (Supplementary Table S1) were chosen for further analyses.

Mathematical modeling

The Hes7 level of cell i is described by $X_i(t)$ (where $i = 1,2,\ldots,36$ and t is time with the unit of hour). Here, τ_1 is the time required for *Hes7* to affect its own formation in the same cell through negative feedback. The interaction between cells is simplified in the following manner. *Dll* is inhibited by *Hes7* in the same cell and activates *Hes7* in other cells. We regard this interaction as the mutual inhibition between two cells with delay τ_2 in *Hes7* dynamics (Extended Data Fig. 9b). Thus, τ_2 represents the time required for *Hes7* from one cell to repress *Hes7* in its neighboring cell. In dynamical equations of the model (Extended Data Fig. 9c), the interpretations of parameters are as follows: v is the maximum synthesis rate; r is the degradation rate; K_1 and K_2 correspond to the typical amounts of HES7 that account for the repression; m and n are the Hill coefficients. $N(i)$ represents the set of cells neighboring to cell i. In numerical simulations, we set $v = 10$, $r = 2$, $K_1 = 1$, $K_2 = 2$, $m = 2$, $n = 2$, $\tau = 0.75$ and observed the dependence of dynamical behavior on τ_2. The same random initial condition was used for all the cases. Note that in parameter space for in-phase oscillation, τ_2 values of longer or shorter than 1.0 results in smaller amplitudes and larger phase differences. τ_2-dependence of oscillation amplitude (X_{amp}) and dispersion

among cells (X_{dis}) are defined as follows. The oscillation amplitude $X_{amp}(i)$ of cell i is defined as the difference between the maximum and minimum $X_i(t)$ values for $t_1 < t < t_2$, where $t_1 = 100$ and $t_2 = 200$. X_{amp} is their average; i.e., $X_{amp} = \frac{1}{36}\sum_{i=1}^{36} X_{amp}(i)$. X_{dis} is the standard deviation of $X_i(t) - \widehat{X}(t)$ for $t_1 < t < t_2$; i.e., $X_{dis} = \sqrt{\frac{1}{36}\sum_{i=1}^{36}\frac{1}{t_2-t_1}\int_{t_1}^{t_2}\{X_i(t) - \widehat{X}(t)\}^2 dt}$. X_{dis} should be compared with X_{amp}; a smaller X_{dis}/X_{amp} value indicates a better synchronization. The oscillation amplitude $X_{amp}(i)$ of cell i is defined as the difference between the maximum and minimum $X_i(t)$ values for $t_1 < t < t_2$, where $t_1 = 100$ and $t_2 = 200$. X_{amp} is their average; i.e., $X_{amp} = \frac{1}{36}\sum_{i=1}^{36} X_{amp}(i)$.

Correspondence and requests for materials should be addressed to Atsushi Miyawaki (matsushi@brain.riken.jp) for Achilles cDNA and Ryoichiro Kageyama (rkageyam@infront.kyoto-u.ac.jp) for the other materials.

Code availability

Image processing and analysis were performed using Fiji(v1.0) and Matlab(R2018a). Subsequent analysis was performed on custom Matlab scripts. The codes are available upon request from the authors.

Data availability

The nucleotide sequence for Achilles cDNA has been deposited in the DDBJ/EMBL/GenBank under the accession number LC381432. Raw data for all experiments are available on request from the authors.

31. Shimizu, Y. *et al.* Cell-free translation reconstituted with purified components. *Nat. Biotechnol.* **19**, 751-5 (2001).
32. Takashima, Y., Ohtsuka, T., González, A., Miyachi, H. & Kageyama, R. Intronic delay is essential for oscillatory expression in the segmentation clock. *Proc. Natl. Acad. Sci. USA* **108**, 3300-3305 (2011).

33. Abe T, Kiyonari H, Shioi G, Inoue K, Nakao K, Aizawa S, Fujimori T. Establishment of conditional reporter mouse lines at ROSA26 locus for live cell imaging. *Genesis* **49**, 579-590 (2011).
34. Tinevez JY, Perry N, Schindelin J, Hoopes GM, Reynolds GD, Laplantine E, Bednarek SY, Shorte SL, Eliceiri KW. TrackMate: An open and extensible platform for single-particle tracking. *Methods* **115**,80-90 (2016).
35. Webb, A.B., Lengyel, I.M., Jörg, D.J., Valentin, G., Jülicher, F., Morelli, L.G. & Oates, A.C. Persistence, period and precision of autonomous cellular oscillators from the zebrafish segmentation clock. *eLife* **5,** e08438 (2016).
36. Isomura, A. & Kageyama, R. An optogenetic method to control and analyze gene expression patterns in cell-to-cell interactions. *J. Vis. Exp.* **133,** e57149 (2018).

Extended Data Figure legends

Extended Data Figure 1. Loss of *Lfng* affects *Hes7* oscillation dynamics at a tissue level. a. pHes7-UbLuc imaging in WT and *Lfng*-KO PSM. Spatio-temporal patterns along the antero-posterior axis are shown. Top is anterior. **b.** Period of *Hes7* oscillations in the anterior and posterior PSM (n=4). **c.** Amplitude of *Hes7* oscillations (n=4). Error bars indicate SEM. **p*<0.05, unpaired *t* test.

Extended Data Figure 2. Comparative characterization of Achilles vs. Venus. a. Absorption spectra of Achilles (red) and Venus (black). **b.** Fluorescence images of bacteria expressing Achilles and Venus. Bacterial colonies were grown at 37°C and photographed at 8, 12, and 20 h post-transformation. Exactly the same amount of competent bacterial cells was used for transformation. Scale bar, 5 mm. **c.** Time course of fluorescence intensities of transformed *E. coli* colonies (mean values ± SEM from three experiments). The data were normalized to the final yields extrapolated by curve fitting (broken line). **d.** Comparison of properties of Achilles and Venus.

Extended Data Figure 3. Schematic structures of Hes7 fluorescent reporters. a. Venus was inserted between the 5-kb *Hes7* promoter and the *Hes7* gene to drive expression of the Venus-HES7 fusion protein. **b.** Achilles was inserted between the 5-kb *Hes7* promoter and the *Hes7* gene to drive expression of the Achilles-HES7 fusion protein. **c.** Achilles fused to NLS-hPEST is expressed under the control of the *Hes7* promoter. **d.** *Hes7* cDNA without an initiation codon was inserted between the PEST sequence and the *Hes7* 3'UTR of the construct shown in (**c**) to allow the transcripts to mimic endogenous mRNA stability. **e.** The *Hes7* gene (exons + introns) without an initiation codon was inserted between the PEST sequence and the *Hes7* 3'UTR of the construct shown in (**c**). **f.** Achilles fused to NLS-hCL1-hPEST is expressed under the control of the *Hes7* promoter. **g.** *Hes7* cDNA without an initiation codon was inserted between the PEST sequence and the *Hes7* 3'UTR of the construct shown in (**f**).

Extended Data Figure 4. The Achilles-HES7 fusion protein is functional in segment formation. a. Bone and cartilage were stained with Alizarin red and Alcian blue, respectively, at P0. Achilles-Hes7 rescued abnormal vertebra and rib formation in

Hes7-null background. **b.** Higher magnification of thoracic to lumber area in Hes7-Achilles Tg+; *Hes7*-null mouse in **a**. Scale bars, 5 mm.

Extended Data Figure 5. Observation of oscillation dynamics at the single-cell level to analyze the phase coupling mechanism. a. Live imaging (wide field) of a PSM carrying the Hes7-Achilles reporter at E10.5. **b.** Spatio-temporal expression pattern of Hes7-Achilles signals in the PSM (wide field). **c.** A representative cell tracked by Fiji/TrackMate. **d.** A representative phase quantification. Fluorescence time-series from a cell extracted by tracking was converted into phase information by Hilbert transform. **e.** HES7 oscillation phase color-mapped onto the original image. Scale bars, 100 μm.

Extended Data Figure 6. Synchronization of HES7 oscillation in tail bud tissue cultures. a. Hes7-Achilles expression in WT and *Lfng*-KO tail bud tissue cultures. Scale bar, 100μm. **b.** Mean intensity of Hes7-Achilles fluorescence in whole area. **c.** Examples of Hes7-Achilles intensity time-series from single-cell tracking data. **d,e.** Average period (**d**) and amplitude (**e**) of HES7 oscillation at a single-cell level. More than 25 cells for each genotype (control and two independent reporter lines) were examined. N= number of peak pairs used for quantification. Error bars indicate SEM. *p<0.05, unpaired t test. **f.** Distribution of phase in single-cell at the timing of peaks in mean intensity time-series in tail bud cultures. Control and two independent reporter lines were examined. The number of cells examined (N) is indicated. ***p < 0.001, Rayleigh test. **g.** Kuramoto order parameter calculated using Ahilles-Hes7 oscillation phase quantified in **f**. Error bars indicate SEM. *p<0.05, unpaired t test.

Extended Data Figure 7. Acute inhibitor/knockdown treatment of tail bud and dissociated PSM cell cultures. a-c. Hes7-Achilles expression in WT tail bud tissue cultures treated with DMSO control (grey bars) or the Notch inhibitor DAPT (red bars). Period (**a**), amplitude (**a**), and synchrony (**c**) of HES7 oscillations were quantified. Error bars indicate SEM. *p<0.05, unpaired t test. The number of cells examined (N) is indicated. ****p< 0.0001, Rayleigh test. **d.** Kuramoto order parameter calculated using Ahilles-Hes7 oscillation phase quantified in **c** (t400-800 min). Error bars indicate SEM. *p<0.05, unpaired t test. **e,f.** Hes7-Achilles expression in WT tail bud tissue cultures treated with scrambled shRNA (grey bars) or two different *Lfng* shRNAs (blue bars).

Synchrony (**e**) and Kuramoto order parameter (**f**, t600-900 min) of HES7 oscillations were quantified. The number of cells examined (N) is indicated. ****$p< 0.0001$, Rayleigh test. Error bars indicate SEM. *$p<0.05$, unpaired *t* test. **g,h.** Hes7-Achilles expression in dissociated PSM cell cultures treated with DAPT. Period (**g**) and amplitude (**h**) of HES7 oscillations were quantified. Error bars indicate SEM.

Extended Data Figure 8. Mixed cultures of wild-type PSM cells and those carrying a faster *Hes7* oscillator. WT (period = 126.6 ± 2.0 min) and mutant (In(3)) PSM cells that carry a faster *Hes7* oscillator (period = 115.4 ± 1.1 min)[23] were mixed as a minority in mutant or WT cells at 1:20 ratio, and fluorescence in the minority and majority cells was quantified over time. **a.** A small ratio (1:20) of In(3) cells were mixed into an In(3) population. **b.** A small ratio (1:20) of In(3) cells were mixed into a WT population. **c.** A small ratio (1:20) of WT cells were mixed into an In(3) population. The distribution of phase difference between the minority cells and their neighboring cells was calculated at each time point. At least 100 cells were examined for each genotype. ****$p< 0.0001$, Rayleigh test.

Extended Data Figure 9. Mathematical modeling and simulation. a. System geometry. We consider 6 x 6 cells forming a hexagonal lattice with nearest neighbor coupling. **b.** Schematic of the mathematical model. **c.** Dynamical equations of the model. **d.** Time series of $X_i(t)$ for different τ_2 values. The dashed line is the average Hes7 level, i.e., $\widehat{X}(t) = \frac{1}{36}\sum_{i=1}^{36} X_i(t)$. Note that in parameter space for in-phase oscillation, τ_2 values of longer or shorter than 1.0 results in smaller amplitudes and larger phase differences. **e.** τ_2-dependence of oscillation amplitude (X_{amp}) and dispersion among cells (X_{dis}). The oscillation period is also shown.

Extended Data Figure 10. KY02111 partially rescued the amplitude and synchrony of HES7 oscillations in *Lfng*-KO PSM cells. a. Effect of Wnt signaling-related chemical compounds on DLL1-Notch signaling delay was examined by a sender/receiver assay in C2C12 cells. Representative time-series of the *Hes1* reporter signal in receiver cells after light induction of *Dll1* in the presence of DMSO, KY02111, Kenpaullone, or Norcantharidin are shown. **b**. Peak-timings of the *Hes1* reporter after

blue light stimulation. N>10 for each condition. **c**. Fold change of amplitude of the *Hes1* reporter after blue light stimulation. n>10 for each condition. Error bars indicate SEM. *p<0.05, unpaired *t* test. **d.** Quantification of Hes7-Achilles signals in central area (harboring posterior PSM identity) of WT and *Lfng*-KO tail bud cultures in the presence of 0.1% DMSO (control), KY02111, Kenpaullone, or Norcantharidin. **e.** Distribution of phase in single-cell at the timing of peaks in mean intensity time-series in *Lfng*-KO tail bud cultures in the presence of DMSO (control) or KY02111. The number of cells examined (N) is indicated. ***p < 0.001, ****p < 0.0001, Rayleigh test. **f.** Average amplitude of HES7 oscillations in *Lfng*-KO tail bud cultures in the presence of DMSO (control) or KY02111. Error bars indicate SEM. *p<0.05, unpaired *t* test. **g.** Kuramoto order parameter calculated using Ahilles-Hes7 oscillation phase quantified in **e**. Error bars indicate SEM. *p<0.05, unpaired *t* test.

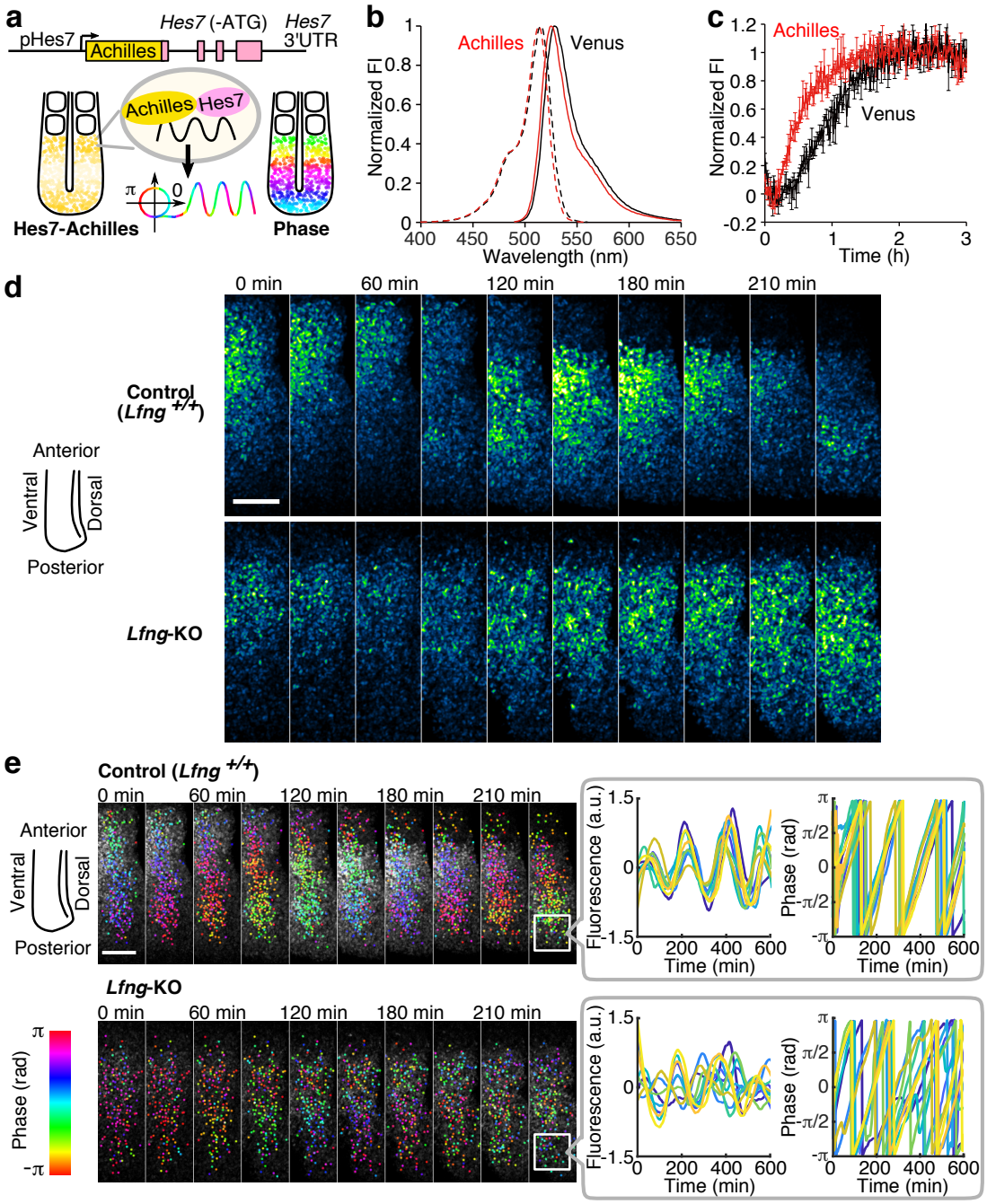
a
pHes7
Achilles
Hes7 (-ATG)
Hes7 3'UTR
Achilles Hes7
π
0
Hes7-Achilles
Phase
b
Achilles
Venus
Normalized FI
Wavelength (nm)
c
Achilles
Venus
Normalized FI
Time (h)
d
0 min
60 min
120 min
180 min
210 min
Control (Lfng +/+)
Anterior
Ventral
Dorsal
Posterior
Lfng-KO
e
Control (Lfng +/+)
0 min
60 min
120 min
180 min
210 min
Anterior
Ventral
Dorsal
Posterior
Lfng-KO
Phase (rad)
Fluorescence (a.u.)
Time (min)

Figure 1

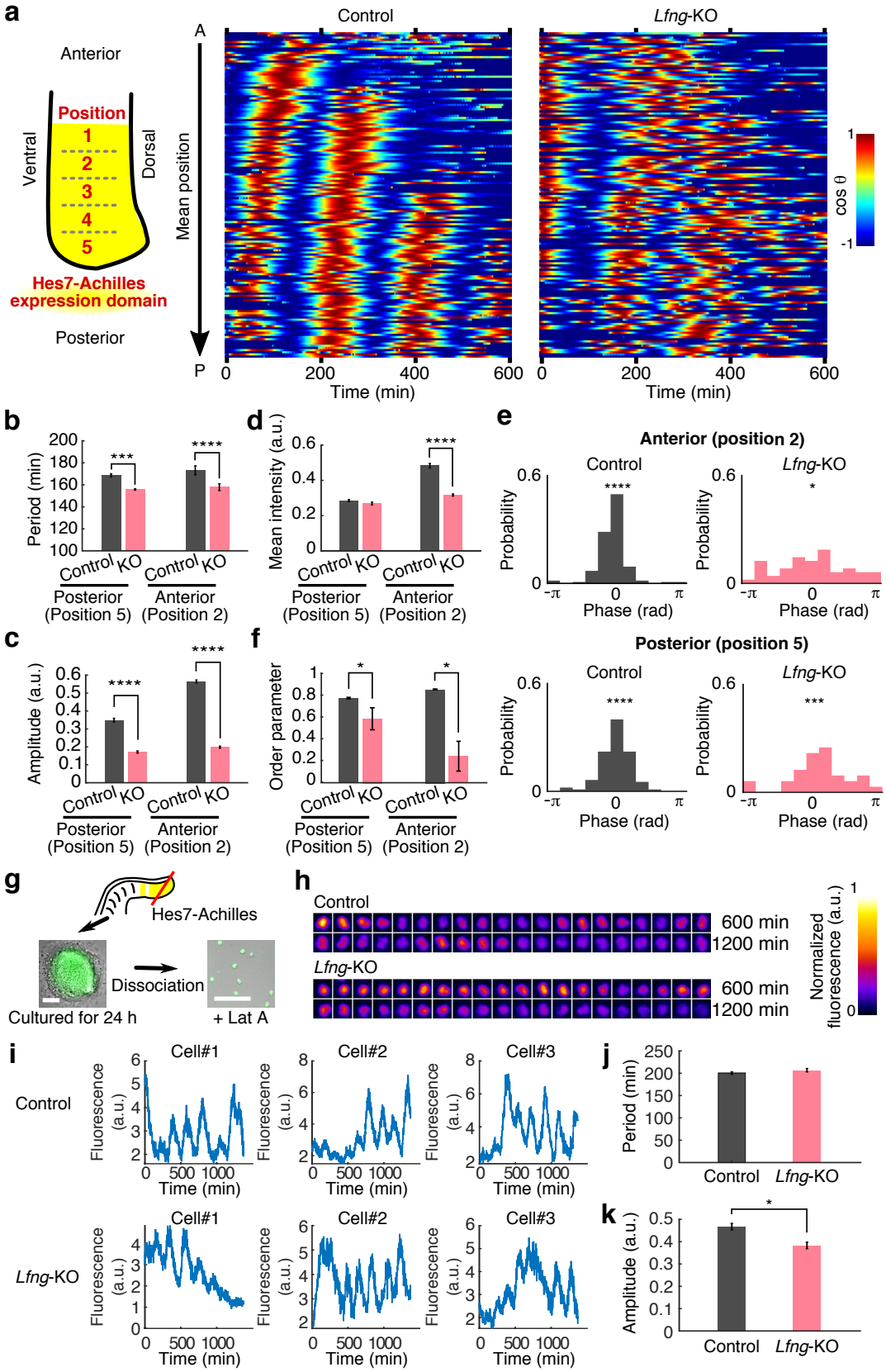
a
Anterior
Position
1
2
3
4
5
Ventral
Dorsal
Hes7-Achilles expression domain
Posterior
A
P
Mean position
Control
Lfng-KO
Time (min)
cos θ
b
Period (min)
Control
KO
Posterior (Position 5)
Anterior (Position 2)
c
Amplitude (a.u.)
d
Mean intensity (a.u.)
e
Anterior (position 2)
Posterior (position 5)
Probability
Phase (rad)
f
Order parameter
g
Hes7-Achilles
Dissociation
Cultured for 24 h
+ Lat A
h
600 min
1200 min
Normalized fluorescence (a.u.)
i
Cell#1
Cell#2
Cell#3
Fluorescence (a.u.)
j
Period (min)
k
Amplitude (a.u.)

Figure 2

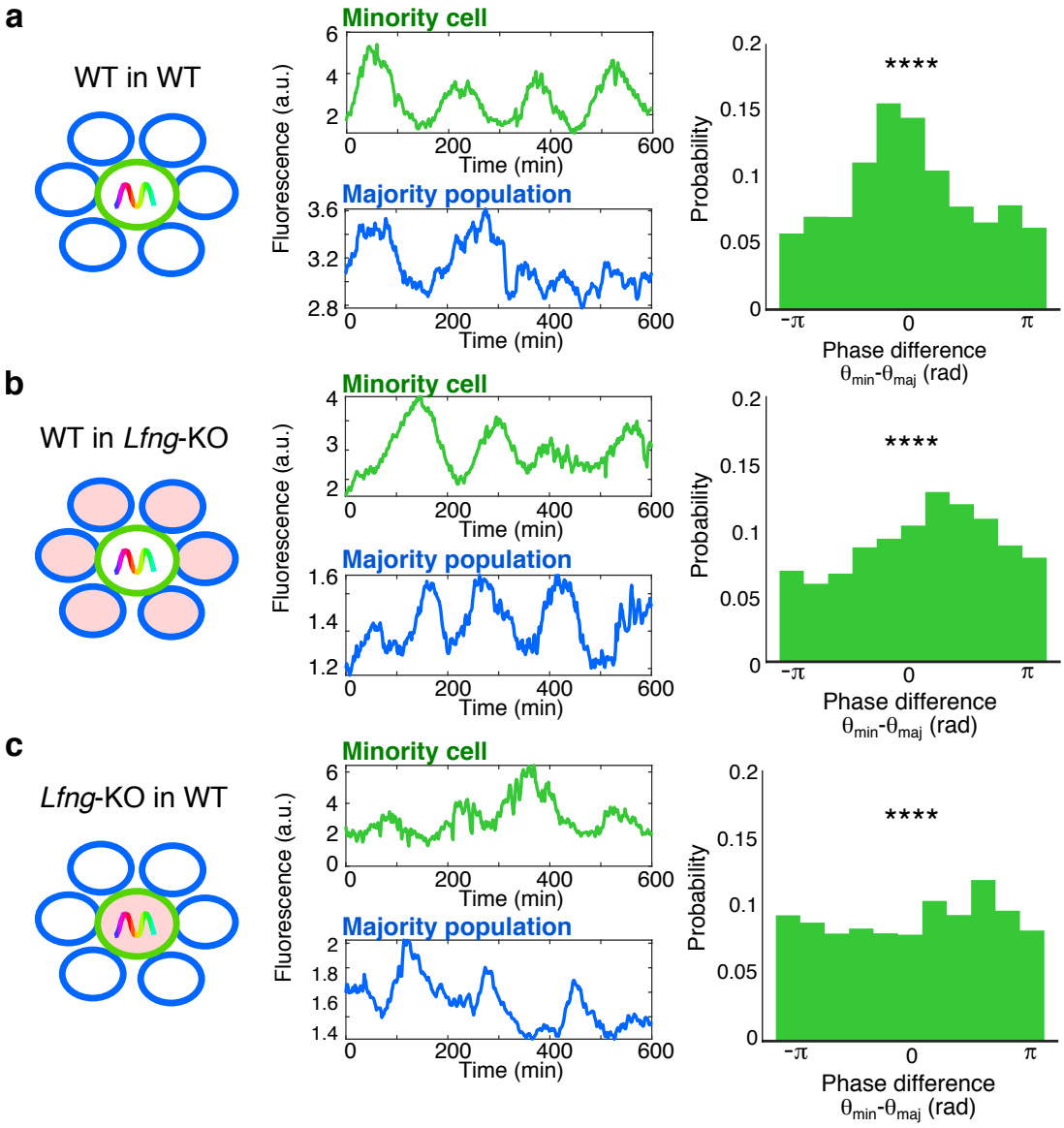
a
WT in WT
Minority cell
Majority population
Fluorescence (a.u.)
Time (min)
Probability
****
Phase difference
θmin-θmaj (rad)
b
WT in Lfng-KO
Minority cell
Majority population
Fluorescence (a.u.)
Time (min)
Probability
****
Phase difference
θmin-θmaj (rad)
c
Lfng-KO in WT
Minority cell
Majority population
Fluorescence (a.u.)
Time (min)
Probability
****
Phase difference
θmin-θmaj (rad)

Figure 3

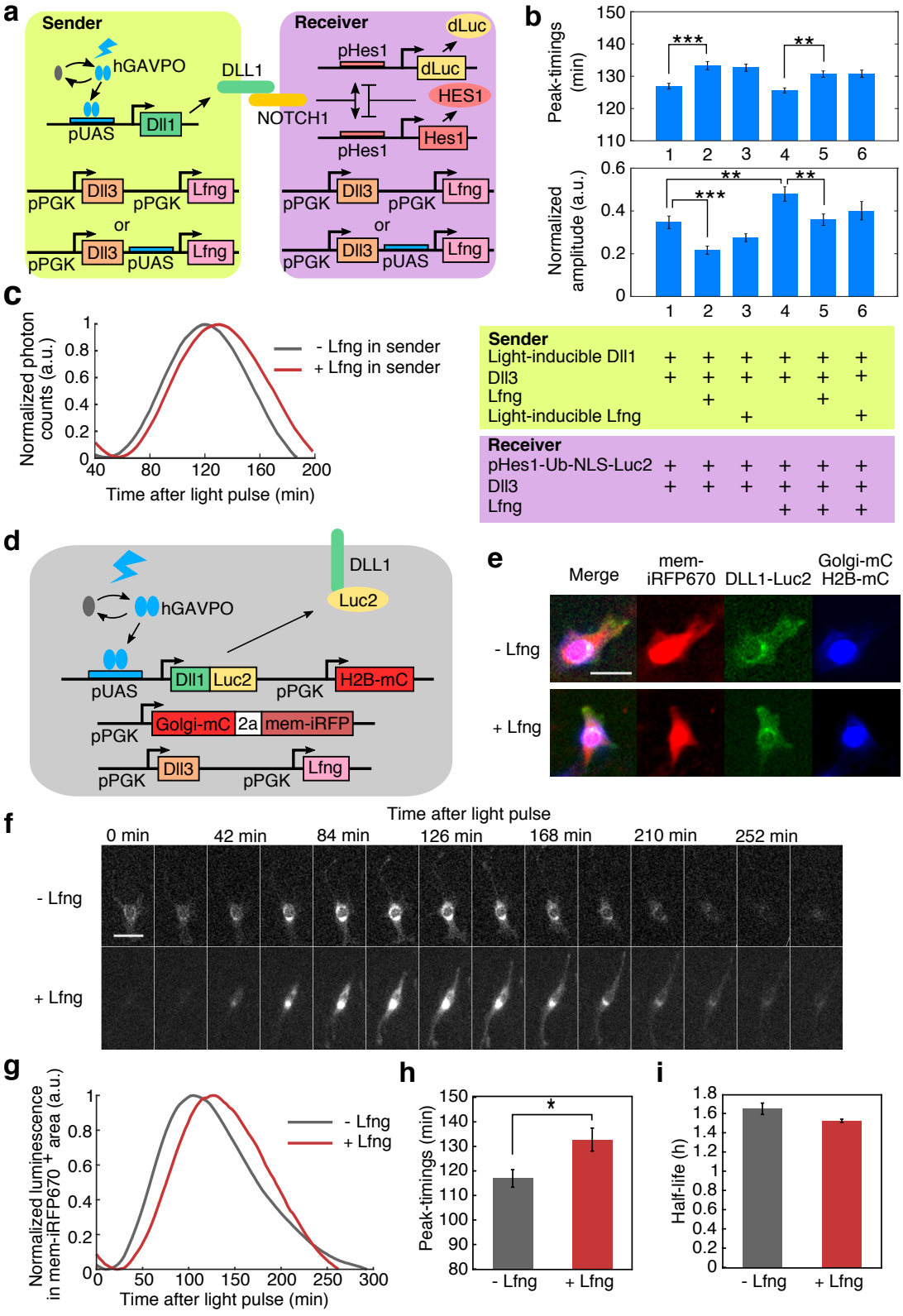
a
Sender
hGAVPO
pUAS
Dll1
DLL1
NOTCH1
Receiver
dLuc
pHes1
HES1
Hes1
pPGK
Dll3
Lfng
or
pUAS
b
Peak-timings (min)
Normalized amplitude (a.u.)
c
Normalized photon counts (a.u.)
- Lfng in sender
+ Lfng in sender
Time after light pulse (min)
Sender
Light-inducible Dll1
Dll3
Lfng
Light-inducible Lfng
Receiver
pHes1-Ub-NLS-Luc2
Dll3
Lfng
d
DLL1
Luc2
hGAVPO
pUAS
Dll1
Luc2
pPGK
H2B-mC
Golgi-mC
2a
mem-iRFP
e
Merge
mem-iRFP670
DLL1-Luc2
Golgi-mC H2B-mC
- Lfng
+ Lfng
f
Time after light pulse
0 min
42 min
84 min
126 min
168 min
210 min
252 min
- Lfng
+ Lfng
g
Normalized luminescence in mem-iRFP670+ area (a.u.)
- Lfng
+ Lfng
Time after light pulse (min)
h
Peak-timings (min)
- Lfng
+ Lfng
i
Half-life (h)
- Lfng
+ Lfng

Figure 4